Title

Identification of a Human Airway Epithelial Cell Subpopulation with Altered Biophysical, Molecular, and Metastatic Properties

Journal

Cancer Prevention Research, 10(9)

ISSN

1940-6207

Authors

Pagano, Paul C

Tran, Linh M

Bendris, Nawal

et al.

Publication Date

2017-09-01

DOI

10.1158/1940-6207.capr-16-0335

Peer reviewed

HHS Public Access

Author manuscript

Cancer Prev Res (Phila). Author manuscript; available in PMC 2018 September 01.

Published in final edited form as:

Cancer Prev Res (Phila). 2017 September ; 10(9): 514–524. doi:10.1158/1940-6207.CAPR-16-0335.

Identification of a human airway epithelial cell subpopulation with altered biophysical, molecular, and metastatic properties

Paul C. Pagano[4], **Linh M. Tran**[1,2], **Nawal Bendris**[10], **Sean O'Byrne**[6], **Henry T. Tse**[6], **Shivani Sharma**[5,7], **Jonathan W. Hoech**[1,2], **Stacy J. Park**[1,2], **Elvira L. Liclican**[1,2], **Zhe Jing**[1,2], **Rui Li**[4], **Kostyantyn Krysan**[1,2], **Manash K. Paul**[1,2], **Yari Fontebasso**[1,2], **Jill E. Larsen**[11], **Shaina Hakimi**[1,2], **Atsuko Seki**[3], **Michael C. Fishbein**[3], **James K. Gimzewski**[5,7], **Dino Di Carlo**[6,7,8], **John D. Minna**[12], **Tonya C. Walser**[1,2,*], and **Steven M. Dubinett**[1,2,3,4,7,8,9,*]

[1]Division of Pulmonary and Critical Care Medicine, David Geffen School of Medicine at UCLA, Los Angeles, CA

[2]Department of Medicine, David Geffen School of Medicine at UCLA, Los Angeles, CA

[3]Department of Pathology and Laboratory Medicine, David Geffen School of Medicine at UCLA, Los Angeles, CA

[4]Department of Molecular and Medical Pharmacology, David Geffen School of Medicine at UCLA, Los Angeles, CA

[5]Department of Chemistry and Biochemistry, UCLA, Los Angeles, CA

[6]Department of Bioengineering, UCLA, Los Angeles, CA

[7]California NanoSystems Institute, Los Angeles, CA

[8]Jonsson Comprehensive Cancer Center, Los Angeles, CA

[9]VA Greater Los Angeles Health Care System, Los Angeles, CA

[10]Department of Cell Biology, UT Southwestern Medical Center, Dallas, TX

[11]QIMR Berghofer Medical Research Institute, Brisbane, Queensland, Australia

[12]Hamon Center for Therapeutic Oncology Research and Departments of Medicine and Pharmacology, UT Southwestern Medical Center, Dallas, TX

Abstract

Lung cancers are documented to have remarkable intratumoral genetic heterogeneity. However, little is known about the heterogeneity of biophysical properties, such as cell motility, and its relationship to early disease pathogenesis and micrometastatic dissemination. In this study, we identified and selected a subpopulation of highly migratory premalignant airway epithelial cells that were observed to migrate through microscale constrictions at up to 100-fold the rate of the

Corresponding author: Steven M. Dubinett, MD, **Address**: Division of Pulmonary and Critical Care Medicine, David Geffen School of Medicine at UCLA, 37-131 Center for Health Sciences Building, 10833 Le Conte Avenue, Los Angeles, CA 90095, **Phone**: 310-267-2725, **Fax**: 310-267-2829, sdubinett@mednet.ucla.edu.

*denotes that TC Walser and SM Dubinett are joint senior authors

Conflicts of interest: The authors declare no conflicts of interest.

unselected immortalized epithelial cell lines. This enhanced migratory capacity was found to be Rac1-dependent and heritable, as evidenced by maintenance of the phenotype through multiple cell divisions continuing more than 8-weeks post-selection. The morphology of this lung epithelial subpopulation was characterized by increased cell protrusion intensity. In a murine model of micrometastatic seeding and pulmonary colonization, the motility-selected premalignant cells exhibit both enhanced survival in short term assays and enhanced outgrowth of premalignant lesions in longer term assays, thus overcoming important aspects of "metastatic inefficiency." Overall, our findings indicate that among immortalized premalignant airway epithelial cell lines, subpopulations with heritable motility-related biophysical properties exist, and these may explain micrometastatic seeding occurring early in the pathogenesis of lung cancer. Understanding, targeting, and preventing these critical biophysical traits and their underlying molecular mechanisms may provide a new approach to prevent metastatic behavior.

Keywords

micropore selection; motility; migration; deformability; EMT; micrometastatic dissemination; metastatic inefficiency

Introduction

The most effective therapy for early stage lung cancer is surgical resection, however, approximately 30% of patients will eventually succumb to metastatic disease following surgery (1). Thus, micrometastatic disease may already be present at the time of surgery, but below the level currently required for clinical detection. This is consistent with the reports of circulating tumor cells in patients with Stage I non-small cell lung cancer (NSCLC) (2, 3). Although metastatic behavior is often considered a late event, these findings: 1) suggest that the metastatic process may be also operative in some patients with early stage disease and 2) are consistent with laboratory-based investigations indicating that dissemination may occur during early tumor development, particularly in the context of epithelial-mesenchymal transition (EMT) (4–8).

A major question is whether all cells within a tumor are capable of metastasis or whether this crucial property resides in only a subset of cells, thus representing clinically important intratumoral heterogeneity. This question also applies to premalignancy, as it has recently been theorized that cells within premalignant lesions may have metastatic capacity (6). While cells derived from a clonal population can vary widely in their gene expression profile (9), an important and often overlooked level of heterogeneity relates to cellular biophysical properties that can regulate stiffness, motility, and migration. Cell stiffness correlates with metastatic potential in a variety of malignancies (10–14), and recent attempts to isolate highly deformable cells established an association between deformability and breast cancer stem cell phenotypes (15). Attempts have been made to isolate cells based on motile behavior *in vitro* or *in vivo* (16, 17). While these studies yielded important findings, critical questions remain unanswered, including: 1) is migration a heritable property?, 2) can subpopulations of cells with inherent migratory capacity be isolated in the absence of chemotactic gradients?, 3) how does enhanced migration relate to factors such as cell

deformability?, 4) what genes are deregulated in migratory epithelial cells, particularly during the earliest stages of carcinogenesis?, and 5) does the highly migratory subpopulation have the capacity for enhanced metastatic potential?

Unlike cancer cells, immortalized human bronchial epithelial cells (HBECs) have been shown to be a genetically stable and robust model of the pulmonary airway epithelium and its associated malignant transformation (18–22). Here, we describe phenotypic heterogeneity among a starting population of immortalized HBECs that prompted our selection (or enrichment) of a distinct subpopulation of highly migratory airway epithelial cells. Micropore selection of these cultured target cells (and controls), followed by their functional, biomechanical, and genetic interrogation, is the focus of the current investigation. Our findings provide insight into the molecular drivers of epithelial cell migration that may ultimately facilitate clinical intervention during the earliest stages of lung cancer development and dissemination.

Materials and Methods

General Cell Culture

Each parental HBEC line was derived from the large airway of an individual patient and immortalized in the absence of viral oncogenes, as previously described (21). The demographics and clinical characteristics of the patients from whom the parental HBEC lines were derived are recorded in Table S1, along with key cell culture characteristics. These HBECs have been well characterized in 2D, 3D, and *in vivo*, where they maintain the capacity for differentiation (18–22). They comprise at least some of the progenitors for human lung cancer, most accurately recapitulating central airway differentiation and squamous cell carcinoma development under the defined culture conditions we utilize. Detailed information about the generation of HBEC-vector and -Snail lines was previously published, along with detailed cell culture maintenance methods (23). All cells were genotyped by STR profiling (DNA IQ System and Powerplex 1.2 system, Promega) before and after migration selection at the UCLA Genotyping and Sequencing Core. They were used within 10 passages of authentication and routinely tested to be free of mycoplasma contamination (MycoAlert, Lonza).

Western Blot

Western blots were performed according to standard procedures. Horseradish peroxidase-conjugated secondary antibodies (Bio-Rad, Hercules, CA) and enhanced chemiluminescence (ECL) reagent (Amersham Biosciences, Piscataway, NJ) were used for protein detection. Primary antibodies were from the following sources: TUBULIN and SNAIL (Cell Signaling Technologies, Danvers, MA); RHOA and RAC1 (Cytoskeleton Inc, Denver, CO). Densitometry was performed in ImageJ using the “analyze gels” function.

Transwell migration assay

Cells were seeded into the top chamber of 12-well format Millicell inserts at 75,000 cells/well in 0.5 mL complete medium (Millipore, Billerica, MA) and incubated at 37°C. Media in both chambers were replaced after 24 hours. After 48 hours, the transwells were swabbed,

fixed in 4% Paraformaldehyde (PFA), and stained with Hoechst-33342 (Molecular Probes). Plating density was determined in un-swabbed transwells by staining with Hoechst and imaging the entire well at 40× total magnification on a Nikon Eclipse Ti inverted microscope (Nikon 4× PlanFluor PhL DL 0.13 NA). Images were captured on a 1024×1024 pixel Cascade II EM-CCD camera with equal exposure times using Nikon Elements AR software. Cell density was determined by fluorescence intensity using the "histogram" function in ImageJ. Cell counts described below were normalized to fluorescence intensity of the respective well. To determine the number of cells that entered the bottom chamber, cells were simultaneously stained with NucRed Live647 (stains all cells) and 1μg/mL DAPI for 20 minutes in complete medium at 37°C (Life Technologies). After staining, the cells were washed and fixed with 4% PFA. Within two hours of staining, images of at least 25 fields in each well were captured using a 10× objective (Nikon PlanFluor Ph1 DLL 0.30 NA). The cells were enumerated using the "threshold" and "analyze particles" functions in ImageJ. Viability is reported as total cells minus dead cells, divided by total cells.

Selection of highly migratory cells

Cells (300,000 per well) were seeded in 6-well format Millicell inserts in 2 mL medium. Media in both chambers were replaced after 24 hours. After 48 hours, cells in the bottom chamber alone were harvested (trypsinization at 37°C followed by centrifugation and resuspension in medium), and the cells were added to the bottom chamber of the original plate. Cells were expanded and plated for a subsequent round of selection. dditional selection pressure was applied by selecting the cells for three rounds through 8 μm pores, then three rounds through 5 μm pores, and finally five rounds through 3 μm pores. Thus, velocity/migration was the first-order selection method applied at every passage, and deformability was the second-order selection method applied only at the two pore size steps (from 8um-to-5um and from 5um-to-3um).

Gene expression analysis

After phenotypic validation, these highly migratory cells (and control cells) were profiled using Affymetrix GeneChip HTA 2.0 gene arrays at the UCLA Clinical Microarray Core. The raw data have been deposited at National Center for Biotechnology Information's (NCBI) gene expression omnibus (GEO) (accession GSE100527). Gene level normalization was performed using the Affymetrix Expression Console and the RMA approach. Non-annotated transcripts were then filtered out from the data before further analysis. Bioconductor *limma* package was used for gene expression analysis. A gene was defined as being differentially expressed if two conditions were met: (1) its fold change was greater than 1.5 and (2) its two-tail t-test p-value was less than 0.1. Cluster 3.0 was used for clustering analysis. Gene set enrichment analysis (GSEA) was used for identifying deregulated pathways and biological processes associated with deregulated genes (29).

Inverted invasion assay

This specialized invasion assay was performed according to previously published protocols (24, 25). Assays were performed in 96-well plates (Black wells, clear bottom, PerkinElmer). Briefly, ice-cold serum-free liquid bovine collagen (PureCol) was prepared at 1 mg/ml concentration. After trypsinization, the cells were added to the collagen suspension at a final

concentration of 5×10^4cells/ml, and 100 μl aliquots were dispensed into five replicate wells. The cells were subsequently spun down, then incubated in a 37°C/5% CO2 tissue-culture incubator to allow the collagen to solidify. Finally, the collagen plug was covered by 30 μl of a mixture of the appropriate culture medium diluted 1:1 with PBS. After 48 hours, the cells were fixed with 4% PFA (final concentration) and stained with 10 μg/ml Hoechst-33342. Images of nuclei staining were obtained on an inverted microscope operated by Nikon Elements Software using a 20× air objective. Twenty-five adjacent images covering ~85% of the well area were taken from 0 μm (bottom of the plate) to 150 μm up in the collagen plug, at 25 μm steps. Quantification of nuclei/well was obtained using the "object count" feature of Nikon Elements Software. Invasion ratio was calculated as the sum of cell counts at 50, 75, 100, 125 and 150 μm over cell counts at 0 μm.

Deformability Cytometry (DC)

The deformability cytometry (DC) microfluidic devices were fabricated following standard polydimethylsiloxane (PDMS) replica molding techniques (26). Documented channel design schematics were also followed for the DC chip master molds (27). Dissociated cell samples were diluted with media to achieve a concentration between 100,000–200,000 cells/mL and introduced to the DC chip at 800 μL/min using a Harvard Apparatus syringe pump. Additional details on experimental design and post-processing analysis are available in previous reports (27) and in supplementary methods.

Micrometastatic seeding and lung colonization model in NSG mice

Pathogen-free NOD.Cg-*Prkdc*^{scid} *Il2rg*^{tm1Wjl}/SzJ (NOD *scid* gamma or NSG) mice were purchased from Jackson Labs and maintained in the UCLA Biocontainment Facility. All studies were approved by the institution's animal review committee (ARC #2011-084). Cells were harvested and washed twice with sterile saline, then suspended at a concentration of 5×10^5 cells in 50 μL for injection into the lateral tail vein of restrained mice. The mice were euthanized by CO_2 asphyxiation at one of two time points—early (72 hours) or late (26–74 days). The lungs from each mouse were harvested and divided into two work flows (qPCR or IHC) that allow quantitation of human HBEC cells within mouse tissues; the left lung was always utilized for qPCR and the right lungs for IHC. For qPCR analysis, genomic DNA was isolated using the DNeasy Blood & Tissue Kit (Qiagen, Limburg, Netherlands). The percentage of human cells (HBECs) relative to the number of mouse cells (host lung) in each sample was determined using the primers and qPCR conditions previously described (28), with the exception that 100 ng of input DNA was used here. For IHC analysis, the mouse organs were fixed in 10% neutral buffered formalin for 48hr before being rinsed thoroughly and transferred to 70% ethanol. The tissues were then processed routinely, sectioned, H&E stained, and immunostained using standard methods previously described (23). Detection of single cells or small aggregates of HBECs within the mouse lungs was confirmed by CD44 (Cell Signaling #3570) immunostaining at 1:400 in EDTA with antigen retrieval. CD44+ HBECs within the murine lungs were manually counted and normalized to the total lung area stained. Representative photomicrographs were obtained using an Olympus BX50 microscope, with Plan APO objective lenses, an Olympus DP21 camera, and Olympus Camedia software.

Fluorescence Microscopy

Cells were grown on 12 mm glass coverslips (Electron Microscopy Sciences, Hatfield, PA) in complete medium. Cells were fixed and permeabilized using 4% PFA and 0.1% Triton X-100 using standard methods. Cells were blocked for 30 minutes in 1% BSA. For nuclear size determination, cells were labeled in blocking buffer with 1:1000 mouse anti-Lamin B1 (AbCAM, Cambridge, MA) for 30 minutes at room temperature. Cells were stained for 30 minutes at room temperature in secondary antibody (goat anti-mouse Alexafluor488, Life Technologies). For cytoskeleton fluorescence, cells were stained with phalloidin-AlexaFluor647 (Life Technologies) and counterstained with DAPI according to the manufacturer's instructions. ProLong Gold (Life Technologies) was used to mount the coverslips. Cells were imaged at room temperature using a Nikon Eclipse 90i upright fluorescent microscope and 10× or 20× objective (Nikon 10× PlanFluor DIC L/N1, 0.30 NA; Nikon 20× Plan Apo VC DIC N2, 0.75 NA). Images were captured using a Nikon Digital Sight DS-Qi1Mc camera at 1024×1024 or 1280×1024 pixel resolution. To quantify nuclear size, the images were thresholded using ImageJ. The "analyze particles" function was used to determine the nuclear area. At least 60 cells of each type were analyzed for nuclear size.

Activated GTPase pull down

Cell lysates were harvested and utilized in a GTPase pull down assay using a commercially available kit according to the manufacturer's instructions (Activation Assay Combo Kit Cytoskeleton Inc, Denver, CO). Additional information can be found in supplementary methods.

Statistical Analysis

Samples were plated and run in triplicate, unless otherwise indicated, and all *in vitro* experiments were performed at least three times. Data represent mean and SEM of one representative experiment, and one representative experiment/image is shown. The statistical significance of these data was determined using a nonpaired Student *t*-test with 95% confidence interval or the Mann-Whitney test (two-tailed, 95% confidence interval) where appropriate. Data were reported significant as follows: * if $P \leq 0.05$, ** if $P \leq 0.01$, and *** if $P \leq 0.001$.

Additional methods are included in the Supplementary methods section.

Results

Highly migratory epithelial cells can be enriched from a heterogeneous population of HBECs and exhibit heritability of this phenotype

Among unselected HBEC cell lines, our observation of a phenotypically distinct cell type that was highly migratory relative to its neighbors, suggested that there is intrinsic heterogeneity in the starting population of cells that could be relevant to dissemination. Approximately 1 in 10,000 of the unselected immortalized HBEC cells was phenotypically distinct (FIG S1a). To isolate these rare highly migratory pulmonary epithelial cells, we devised a selection strategy using a series of microporous membranes (FIG 1a). Cells were initially seeded on 8 μm-pore transwell membranes with basal medium in the top and bottom

chambers and allowed to migrate for 48 hours. Chemotactic gradients were avoided to minimize induction of directed motility and selection based on this phenotype. To avoid inadvertent generation of a gradient due to nutrient depletion, media in both chambers were replaced after 24 hours. The cells in the bottom chamber were isolated by trypsinization and propagated in a new dish. They were re-plated onto a new membrane, and the process was repeated. To further increase selection pressure, the pore size was serially decreased, first to 5-μm and then 3-μm pores. It is noteworthy that an insufficient quantity of viable cells migrated through 5- or 3 μm pores within 48 hours to justify immediate selection at these sizes, thus negating the possibility of skipping *a priori* selection through 8 μm pores. Cells selected based on their migratory capacity are denoted HM (highly migratory), and they were compared to the unselected starting population in all subsequent studies (FIG 1b).

The HM cells were subjected to a migration assay using 8, 5, and 3 μm pore membranes and stained to quantify the migration rate. Selected HBEC3 with p53 deletion and KRAS activating mutation (H3PK-HM) had a 5-fold higher migration rate through 8 μm pores, a 30-fold higher migration rate through 5 μm pores, and a 124-fold higher migration rate through 3 μm pores, compared to their unselected counterparts; similar trends were observed for H3-HM and H4-HM cell lines (FIG 2a, Table S2). Additional cellular processes are required for invasion, thus we sought to determine if the highly migratory cells were also highly invasive. H3-HM and H4-HM cells showed enhanced invasion in a collagen matrix compared to parental cells (FIG 2b). H3PK-HM cells showed no difference in invasion through collagen. However, the baseline invasion rate in the H3PK cell line was already high, suggesting that migration was not rate-limiting for these cells in this assay.

To determine if the migratory phenotype would be sustained through many generations, the transwell migration assay was performed 8 weeks post-selection (~40 population doublings). Over this time, the selected cells remained highly migratory relative to their unselected counterparts (FIG 2c), indicating that the selected migration phenotype is heritable and can be exploited to expand the cells for downstream functional analyses.

Biophysical characterization of highly migratory cells reveals a cell protrusion phenotype and no selection bias based on nuclear size

Cells with the capacity to alter their morphology by increasing their cellular protrusions may also have an enhanced ability to conform to constrictive spaces. Images of highly migratory cells were taken using phase contrast microscopy. Using ImageJ (30), outlines were made of each cell (FIG S1b), and the corresponding ratio of perimeter to area was calculated to determine “protrusion intensity”, which relates to the number of protrusions. H3-HM, H4-HM, and H3PK-HM cells all demonstrated increased protrusion intensity (FIG 3a). Recently, it has been suggested that the nucleus can be a rate-limiting factor in successful migration, such that matrix metalloproteinase-independent migration was shown to decline as a linear function of pore size and with deformation of the nucleus, with arrest reached at a pore size of 10% of the nuclear cross-sectional area (31). We measured the nuclear cross-sectional area by imaging cells following nuclear lamin staining, to determine if nuclear size was a factor in the HM cell subpopulation which was selected based on matrix metalloproteinase-independent migration. H4-HM cells have increased nuclear area, while

H3-HM and H3PK-HM cells show no significant difference in nuclear size (FIG 3b). The 3-micron pore size in the migration assay used here is much smaller than 10% of the nuclear cross section of all cell lines in the study, suggesting that nucleus size alone is not a rate limiting factor. The results indicate that our selection strategy does not bias for cells with smaller nuclei, and selects cells based on migrational competence. This increased protrusion intensity suggests that HM cells may have greater control over their morphology, which would facilitate their migration through constrictive spaces.

Determining the association of cell size and deformability in migration

We sought to determine if the micropore selection process co-selected for increased deformability as a consequence of selecting cells capable of migrating through decreasing pore sizes that are a fraction of the cell volume. To assess cellular deformability, we utilized deformability cytometry (DC) (27). This technique uses hydrodynamic forces to stretch cells uniformly in a microfluidic chip, followed by high-speed imaging to discern changes in cell shape and size as a result of applied stress. Deformability (D) is a unitless measure defined as the maximum ratio of the long to short axis of a cell stretched with a standard stress, such that a cell with a lower stiffness will have a corresponding higher deformability. There was no across-the-board increase in deformability as a result of micropore selection (FIG 3c, Table S3). A secondary readout of DC is cell size, measured when the epithelial cells are in suspension just prior to being deformed. As with deformability, cell line-dependent results were also observed for cell size (FIG 3c). This suggests that the selection strategy does not bias towards biophysical properties, such as size or deformability, but rather selects cells based on migratory behavior more specifically.

Selection isolates cells capable of overcoming a critical juncture in metastatic inefficiency

While EMT is known to drive the invasion and metastasis of established tumors (32), it has also been theorized to drive dissemination during lung premalignancy (6). However, the isolated subpopulation of cells did not exhibit morphological characteristics associated with EMT (FIG S1b). To evaluate EMT-related phenomena in our highly migratory model, we performed selection in HBECs that have been genetically engineered to over-express SNAIL (23). Similarly to isogenic cells, enhanced migration was observed in these SNAIL over-expressing HM cells (FIG S2a, Table S2).

By dual staining for live/dead cell analysis, we found that without prior selection, migration through 3 μm pores results in a high incidence of cell death in the H3PK cells, accounting for approximately 50% viability regardless of SNAIL expression level (FIG S2b–c). This explains the need for a two-step selection process (velocity/migration the primary, and deformability the secondary) and indirectly suggests HM cells are better equipped to metastasize to distant sites via their capacity for enhanced survival during migration. Leonard Weiss first described the concept of “metastatic inefficiency,” which has been observed by others (33, 34). It refers to points in the metastatic cascade that typically result in cell death, including 1) intravasation and 2) extravasation (35). These reports and the observations from our post-migration viability studies prompted us to test our selected cells in an *in vivo* model that would examine the second transition from the intravascular space to the lung parenchyma. A key technical limitation of the IV experimental metastasis model is

that the first transition is not evaluable, because the cells are deposited directly into the blood stream. Here specifically, H3PKS or H3PKS-HM cells (5×10^5) were injected into the lateral tail vein of NSG mice. Tissue was collected for analysis after 72hr, matching the timeframe used in the post-migration viability study and allowing sufficient time for clearance of dead cells from the pulmonary vasculature (36). This timeframe allowed us to focus on the extravasation and survival phenotypes, rather than on tumor outgrowth. Total DNA was extracted from the left lung homogenates, and all remaining lung tissue was processed for IHC. A PCR-based method described by Malek *et al* was used to quantify the number of human bronchial epithelial cells that arrested in the mouse lung (28). Mice injected with the micropore-selected H3PKS-HM cells showed greater than 2.5-fold more human DNA in their lungs on average compared to mice injected with unselected H3PKS cells (FIG 4a). We next evaluated the ability of the two cells types to not only survive the initial phase of implantation in the lung, but to survive long term (26–74 days), to extravasate from the vasculature and/or lymphatics, and to successfully colonize the lung niche by expanding to form premalignant lesions or frank tumors. Among those injected with HM cells, 4 of 7 surviving mice showed evidence of human bronchial epithelial cells at the late time point, as measured by qPCR. Conversely, none of the 7 mice injected with unselected H3PKS cells showed evidence of human cells at corresponding time points (data not shown). Utilizing a human-specific CD44 antibody to delineate human cells, IHC analysis of the right lungs of corresponding mice confirmed the presence of more and larger epithelial cells aggregates in the HM mice (FIG 4b). Furthermore, pathology review found that HPKS-HM cell aggregates could be located outside of the capillary/lymphatic beds in the lung parenchyma (FIG S3). Taken together with the *in vitro* viability studies, this suggests that the selected cells are endowed with several properties conducive to micrometastatic dissemination: enhanced extravasation from the vasculature and more robust colonization of the lung niche. Thus, enhanced migration is a biophysical trait that allows premalignant epithelial cells to overcome key aspects of metastatic inefficiency.

Fluorescence microscopy reveals SNAIL-mediated changes to the actin cytoskeleton in pulmonary epithelial cells with the highest migratory potential

The actin cytoskeleton is in large part responsible for cell motility and migration through the coordination of numerous factors influencing actin polymerization and depolymerization, among others. Visualizing F-actin in cells can help determine which molecular processes are active. Thus, we grew selected and unselected cells on cover slips and stained them using fluorescent phalloidin. H3PK-HM and H4-HM cells showed no appreciable difference in F-actin structures (FIG S4); conversely, H3PKS-HM cells showed more F-actin bundles in the lamellipodia than their unselected counterparts (FIG 5a). While H4S–HM cells did not show similar F-actin structures, they display striking changes in morphology and protrusions rich in F-actin (FIG 5a). These results show changes to the cytoskeleton in the subpopulation of highly migratory cells when SNAIL is over-expressed, and suggest increased Rac1 activity, a factor known to drive actin polymerization.

Rac1 activity contributes to the high migratory phenotype and can be pharmacologically inhibited

Rho-family GTPases are major regulators of the actin cytoskeleton, and their signaling facilitates processes such as cell polarity and motility (37). Based on our observations of F-actin, we next determined the activation status of two well-characterized GTPases, RhoA and Rac1, to determine if they are altered in the highly migratory cells. Whole-cell lysates were utilized in a pull-down assay with agarose beads conjugated to Rhotekin or p21-activated kinase binding domain (PAK), which recognize GTP-bound (activated) RhoA or Rac1, respectively. We observed no significant change in RhoA activity, but a 2-fold increase in activated Rac1 (FIG 5b). To verify that enhanced Rac1 activity drives migration in HM cells, we pharmacologically inhibited Rac1 in these cells in a migration assay (using a concentration of 10 μM inhibitor, which did not prevent cell growth) (FIG S5). Inhibition of Rac1 activation by NSC-23766, an inhibitor of a Rac1-specific guanine nucleotide exchange factor (GEF), perturbed cell migration compared to control cells (FIG 5c). Similar results were observed in cell line pairs without ectopic expression of Snail, suggesting that the Rac1 pathway activation is at least partially responsible for the highly migratory phenotype and is operative independent of Snail. More broadly, these results suggest that epithelial motility may be targeted pharmacologically by perturbing the Rac1 pathway.

Gene expression analysis reveals changes attributable to the highly migratory phenotype

Because we and others have shown that SNAIL leads to enhanced motility and migration, we sought to determine if highly migratory cells had greater SNAIL expression than their unselected counterparts. No differences in SNAIL protein levels were detected (FIG S6). To determine how gene expression was altered among HM cells we isolated total RNA from the parental line and HM subpopulation and performed microarray mRNA profiling. The raw data have been made publically available via NCBI's GEO (accession GSE100527), and Table S5 highlights the top gene expression changes charactering highly migratory epithelial cells. Interestingly, the H3-HM, H4-HM and H3PK-HM subpopulations did not show significant changes in epithelial or mesenchymal genes, suggesting that EMT has not occurred in these cells, consistent with the morphological observation described earlier. However, there is a subset of genes up-regulated in the HM subpopulation relative to the parental lines from which they were derived that mimic genes upregulated as a result of SNAIL expression (FIG 6a). Next, we determined if gene expression changes in the HM subpopulation correlated with clinical datasets implicating metastatic disease. Gene set enrichment analysis (GSEA) revealed genes correlated with the highly migratory phenotype were also enriched in clinical gene sets associated with poor overall survival in NSCLC, and recurrent disease in breast cancer and melanoma samples (FIG 6b) (38–40).

Discussion

Among immortalized premalignant airway epithelial cell lines, we have identified a small subpopulation of cells with a highly motile and metastatic phenotype, demonstrated using *in vitro* and *in vivo* methods, and found this phenotype is heritable over 40 population doublings. The highly migratory phenotype is enhanced by Snail expression and requires Rac1 activity regardless of Snail expression levels. This system represents an important new

preclinical model for understanding mechanisms and developing therapeutics. This finding also suggests that a population of premalignant airway epithelial cells are endowed with biophysical properties that enable a profound capacity for high velocity migration.

By isolating highly migratory cells from both parental and SNAIL-overexpressing populations, we were able to study SNAIL-independent and SNAIL-dependent mechanisms of migration. This allowed us to model the SNAIL-mediated EMT program, which is known to drive migratory behavior, and is clinically relevant because SNAIL is present in lung premalignant lesions (41). As determined by deformability cytometry, we found the HM subpopulation derived from the H4 line showed increased cellular deformability. This result is in alignment with other studies showing that migration and metastasis correlate with increased cellular deformability (5, 10, 42). However, increased stiffness in H3-HM and H3PK-HM cells suggests that cellular deformability may not always be requisite for the highly motile phenotype. One explanation for the occasional disconnect between motility and deformability may be technical. Velocity/migration was the first-order selection method applied at every passage (at every pore size). Thus, motility differences between HM and control cells were most pronounced and most consistent across cell lines. Deformability was the second-order selection method applied only at the two pore size steps (8um-to-5um and 5um-to-3um). Thus, deformability differences between HM and control cells were not as large and not as consistent across cell lines as the motility physical characteristic. Differences in deformability among the migration-selected cells may also be explained by patient/HBEC heterogeneity. For example, Liu *et al* have recently described different migration modes exist among cells within a single population, which were ascribed to subtle molecular differences (43). We found that Rac1 activity mediates enhanced migration, and that pharmacologic inhibition of Rac1 activation reduced migration in the selected highly migratory cells. Rac1 activity has been associated with carcinogenesis, EMT, and metastasis, and is being explored as a candidate therapeutic target (44, 45). Genes whose expression were upregulated in our highly migratory cells also correlated with poor overall survival in NSCLC and increased recurrence in breast cancer and melanoma. It could be that recurrence is related to micrometastatic disease present, but not detected, at the time of resection. Prospective studies examining the migratory gene sets in pulmonary premalignancy and its relationship to survival in early stage lung cancer patients are anticipated in future investigations.

Although most previous studies utilize fully malignant cancer cells of tumor origin for identification and characterization of highly migratory cells, investigation of premalignant lesions may be equally important. Vaughan *et al* have identified a pulmonary progenitor cell population capable of mobilizing to regenerate the murine lung epithelium following major injury (46). While a corresponding population in the human lung has yet to be identified, these findings support the existence of a subpopulation of highly motile pulmonary epithelial cells that may play a role in the pathogenesis of lung cancer.

Metastasis is the predominate cause of cancer death (47), and while a tumor is made up of many cancer cells, only a small percentage of these cells become metastatic (17, 48, 49). The current study provides a new approach for investigating subpopulations of premalignant human lung epithelial cells in the context of migratory and metastatic behavior. This affords

the opportunity for systematic interrogation of mechanisms and potential preventive or therapeutic targets for patients at risk for lung cancer.

Supplementary Material

Refer to Web version on PubMed Central for supplementary material.

Acknowledgments

The authors acknowledge Ying Lin for technical assistance, the UCLA Genotyping/Sequencing Core for genotyping and microarray services, and Jessica Byrne for assistance with figure preparation. We thank the Translational Pathology Core Laboratory (TPCL) for histology services. We thank the UCLA Clinical and Translational Science Institute (CTSI), as well as the UCLA California Nanosystems Institute Advanced Light Microscopy/Spectroscopy Cores for microscopy resources.

Support: These studies were supported by funding from the following sources: NIH/NCI #T32-CA009120-36 (SMD), NCI #U01CA152751 (SMD), Department of Defense Congressionally Directed Medical Research Programs #LC130767 (SMD), Department of Veteran Affairs #2I01BX000359-05A1 (SMD), National Center for Advancing Translational Science UCLA CTSI Grant UL1TR000124 (SMD), University of California Tobacco-Related Disease Research Program (TRDRP) #22DT-0005 (PCP) and #20KT-055 (TCW), NCI Lung Cancer SPORE #P50CA70907 (JDM), and the Packard Foundation Fellowship (DDC).

References

1. Endo C, Sakurada A, Notsuda H, Noda M, Hoshikawa Y, Okada Y, et al. Results of long-term follow-up of patients with completely resected non-small cell lung cancer. Ann Thorac Surg. 2012; 93:1061–1068. [PubMed: 22386090]
2. Tanaka F, Yoneda K, Kondo N, Hashimoto M, Takuwa T, Matsumoto S, et al. Circulating tumor cell as a diagnostic marker in primary lung cancer. Clinical Cancer Res. 2009; 15:6980–6986. [PubMed: 19887487]
3. Okumura Y, Tanaka F, Yoneda K, Hashimoto M, Takuwa T, Kondo N, et al. Circulating tumor cells in pulmonary venous blood of primary lung cancer patients. Ann Thorac Surg. 2009; 87:1669–1675. [PubMed: 19463575]
4. Mani SA, Guo W, Liao MJ, Eaton EN, Ayyanan A, Zhou AY, et al. The epithelial-mesenchymal transition generates cells with properties of stem cells. Cell. 2008; 133:704–715. [PubMed: 18485877]
5. Rhim AD, Mirek ET, Aiello NM, Maitra A, Bailey JM, McAllister F, et al. EMT and dissemination precede pancreatic tumor formation. Cell. 2012; 148:349–361. [PubMed: 22265420]
6. Sanchez-Garcia I. The crossroads of oncogenesis and metastasis. N Engl J Med. 2009; 360:297–299. [PubMed: 19144947]
7. Husemann Y, Geigl JB, Schubert F, Musiani P, Meyer M, Burghart E, et al. Systemic spread is an early step in breast cancer. Cancer Cell. 2008; 13:58–68. [PubMed: 18167340]
8. Podsypanina K, Du YC, Jechlinger M, Beverly LJ, Hambardzumyan D, Varmus H. Seeding and propagation of untransformed mouse mammary cells in the lung. Science. 2008; 321:1841–1844. [PubMed: 18755941]
9. Rausenberger J, Kollmann M. Quantifying origins of cell-to-cell variations in gene expression. Biophysical Journal. 2008; 95:4523–4528. [PubMed: 18689455]
10. Cross SE, Jin YS, Tondre J, Wong R, Rao J, Gimzewski JK. AFM-based analysis of human metastatic cancer cells. Nanotechnology. 2008; 19:384003. [PubMed: 21832563]
11. Xu W, Mezencev R, Kim B, Wang L, McDonald J, Sulchek T. Cell stiffness is a biomarker of the metastatic potential of ovarian cancer cells. PLoS One. 2012; 7:e46609. [PubMed: 23056368]
12. Cross SE, Jin YS, Rao J, Gimzewski JK. Nanomechanical analysis of cells from cancer patients. Nature Nanotechnology. 2007; 2:780–783.

13. Guck J, Schinkinger S, Lincoln B, Wottawah F, Ebert S, Romeyke M, et al. Optical deformability as an inherent cell marker for testing malignant transformation and metastatic competence. Biophysical Journal. 2005; 88:3689–3698. [PubMed: 15722433]
14. Lautenschlager F, Paschke S, Schinkinger S, Bruel A, Beil M, Guck J. The regulatory role of cell mechanics for migration of differentiating myeloid cells. Proc Natl Acad Sci U S A. 2009; 106:15696–15701. [PubMed: 19717452]
15. Zhang W, Kai K, Choi DS, Iwamoto T, Nguyen YH, Wong H, et al. Microfluidics separation reveals the stem-cell-like deformability of tumor-initiating cells. Proc Natl Acad Sci U S A. 2012; 109:18707–18712. [PubMed: 23112172]
16. Seo M, Lee WH, Suk K. Identification of novel cell migration-promoting genes by a functional genetic screen. FASEB Journal. 2010; 24:464–478. [PubMed: 19812375]
17. Patsialou A, Wang Y, Lin J, Whitney K, Goswami S, Kenny PA, et al. Selective gene-expression profiling of migratory tumor cells in vivo predicts clinical outcome in breast cancer patients. Breast Cancer Research:BCR. 2012; 14:R139. [PubMed: 23113900]
18. Delgado O, Kaisani AA, Spinola M, Xie XJ, Batten KG, Minna JD, et al. Multipotent capacity of immortalized human bronchial epithelial cells. PLoS One. 2011; 6:e22023. [PubMed: 21760947]
19. Grant JL, Fishbein MC, Hong LS, Krysan K, Minna JD, Shay JW, et al. A novel molecular pathway for Snail-dependent, SPARC-mediated invasion in non-small cell lung cancer pathogenesis. Cancer Prevention Res. 2014; 7:150–160.
20. Kaisani A, Delgado O, Fasciani G, Kim SB, Wright WE, Minna JD, et al. Branching morphogenesis of immortalized human bronchial epithelial cells in three-dimensional culture. Differentiation. 2014; 87:119–126. [PubMed: 24830354]
21. Ramirez RD, Sheridan S, Girard L, Sato M, Kim Y, Pollack J, et al. Immortalization of human bronchial epithelial cells in the absence of viral oncoproteins. Cancer Res. 2004; 64:9027–9034. [PubMed: 15604268]
22. Sato M, Larsen JE, Lee W, Sun H, Shames DS, Dalvi MP, et al. Human lung epithelial cells progressed to malignancy through specific oncogenic manipulations. Mol Cancer Res. 2013; 11:638–650. [PubMed: 23449933]
23. Grant JL, Fishbein MC, Hong LS, Krysan K, Minna JD, Shay JW, et al. A novel molecular pathway for Snail-dependent, SPARC-mediated invasion in non-small cell lung cancer pathogenesis. Cancer Prevention Res. 2013
24. Arsic N, Bendris N, Peter M, Begon-Pescia C, Rebouissou C, Gadea G, et al. A novel function for Cyclin A2: control of cell invasion via RhoA signaling. The Journal of Cell Biology. 2012; 196:147–162. [PubMed: 22232705]
25. Bendris N, Williams KC, Reis CR, Welf ES, Chen PH, Lemmers B, et al. SNX9 promotes metastasis by enhancing cancer cell invasion via differential regulation of RhoGTPases. Mol Biol Cell. 2016
26. Sollier E, Murray C, Maoddi P, Di Carlo D. Rapid prototyping polymers for microfluidic devices and high pressure injections. Lab on a Chip. 2011; 11:3752–3765. [PubMed: 21979377]
27. Gossett DR, Tse HT, Lee SA, Ying Y, Lindgren AG, Yang OO, et al. Hydrodynamic stretching of single cells for large population mechanical phenotyping. Proc Natl Acad Sci U S A. 2012; 109:7630–7635. [PubMed: 22547795]
28. Malek A, Catapano CV, Czubayko F, Aigner A. A sensitive polymerase chain reaction-based method for detection and quantification of metastasis in human xenograft mouse models. Clinical & Experimental Metastasis. 2010; 27:261–271. [PubMed: 20364399]
29. Subramanian A, Tamayo P, Mootha VK, Mukherjee S, Ebert BL, Gillette MA, et al. Gene set enrichment analysis: a knowledge-based approach for interpreting genome-wide expression profiles. Proc Natl Acad Sci U S A. 2005; 102:15545–15550. [PubMed: 16199517]
30. Schneider CA, Rasband WS, Eliceiri KW. NIH Image to ImageJ: 25 years of image analysis. Nature Methods. 2012; 9:671–675. [PubMed: 22930834]
31. Wolf K, Te Lindert M, Krause M, Alexander S, Te Riet J, Willis AL, et al. Physical limits of cell migration: control by ECM space and nuclear deformation and tuning by proteolysis and traction force. The Journal of Cell Biology. 2013; 201:1069–1084. [PubMed: 23798731]

32. Tam WL, Weinberg RA. The epigenetics of epithelial-mesenchymal plasticity in cancer. Nature Medicine. 2013; 19:1438–1449.
33. Weiss L. Cancer cell traffic from the lungs to the liver: an example of metastatic inefficiency. International Journal of Cancer. 1980; 25:385–392. [PubMed: 7390660]
34. Luzzi KJ, MacDonald IC, Schmidt EE, Kerkvliet N, Morris VL, Chambers AF, et al. Multistep nature of metastatic inefficiency: dormancy of solitary cells after successful extravasation and limited survival of early micrometastases. The American Journal of Pathology. 1998; 153:865–873. [PubMed: 9736035]
35. Chambers AF, Naumov GN, Vantyghem SA, Tuck AB. Molecular biology of breast cancer metastasis. Clinical implications of experimental studies on metastatic inefficiency. Breast Cancer Res. 2000; 2:400–407. [PubMed: 11250733]
36. Fidler IJ, Nicolson GL. Organ selectivity for implantation survival and growth of B16 melanoma variant tumor lines. J Natl Cancer Inst. 1976; 57:1199–1202. [PubMed: 1003551]
37. Sit ST, Manser E. Rho GTPases and their role in organizing the actin cytoskeleton. Journal of Cell Science. 2011; 124:679–683. [PubMed: 21321325]
38. Sotiriou C, Wirapati P, Loi S, Harris A, Fox S, Smeds J, et al. Gene expression profiling in breast cancer: understanding the molecular basis of histologic grade to improve prognosis. J Natl Cancer Inst. 2006; 98:262–272. [PubMed: 16478745]
39. Kauffmann A, Rosselli F, Lazar V, Winnepenninckx V, Mansuet-Lupo A, Dessen P, et al. High expression of DNA repair pathways is associated with metastasis in melanoma patients. Oncogene. 2008; 27:565–573. [PubMed: 17891185]
40. Shedden K, Taylor JM, Enkemann SA, Tsao MS, Yeatman TJ, et al. Director's Challenge Consortium for the Molecular Classification of Lung A. Gene expression-based survival prediction in lung adenocarcinoma: a multi-site, blinded validation study. Nature Medicine. 2008; 14:822–827.
41. Walser T, Yanagawa J, Luo J, Liu M, Goodglick L, Hong L-S, et al. Abstract PR-11: Snail-induced and EMT-mediated early lung cancer development: Promotion of invasion and expansion of stem cell populations. Cancer Prevention Res. 2008; 1:PR-11.
42. Tse HT, Gossett DR, Moon YS, Masaeli M, Sohsman M, Ying Y, et al. Quantitative diagnosis of malignant pleural effusions by single-cell mechanophenotyping. Science Translational Medicine. 2013; 5:212ra163.
43. Liu YJ, Le Berre M, Lautenschlaeger F, Maiuri P, Callan-Jones A, Heuze M, et al. Confinement and low adhesion induce fast amoeboid migration of slow mesenchymal cells. Cell. 2015; 160:659–672. [PubMed: 25679760]
44. Radisky DC, Levy DD, Littlepage LE, Liu H, Nelson CM, Fata JE, et al. Rac1b and reactive oxygen species mediate MMP-3-induced EMT and genomic instability. Nature. 2005; 436:123–127. [PubMed: 16001073]
45. Dirat B, Ader I, Golzio M, Massa F, Mettouchi A, Laurent K, et al. Inhibition of the GTPase Rac1 Mediates the Antimigratory Effects of Metformin in Prostate Cancer Cells. Molecular Cancer Therapeutics. 2014
46. Vaughan AE, Brumwell AN, Xi Y, Gotts JE, Brownfield DG, Treutlein B, et al. Lineage-negative progenitors mobilize to regenerate lung epithelium after major injury. Nature. 2015; 517:621–625. [PubMed: 25533958]
47. Reymond N, d'Agua BB, Ridley AJ. Crossing the endothelial barrier during metastasis. Nature Reviews Cancer. 2013; 13:858–870. [PubMed: 24263189]
48. Yokota J. Tumor progression and metastasis. Carcinogenesis. 2000; 21:497–503. [PubMed: 10688870]
49. Sidani M, Wyckoff J, Xue C, Segall JE, Condeelis J. Probing the microenvironment of mammary tumors using multiphoton microscopy. Journal of Mammary Gland Biology and Neoplasia. 2006; 11:151–163. [PubMed: 17106644]

a:

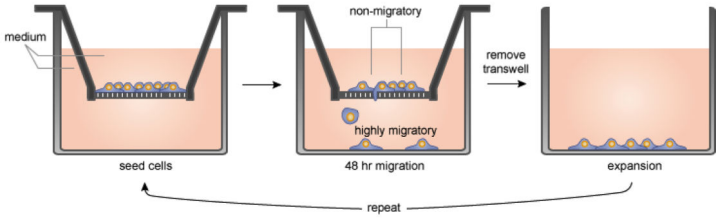

b:

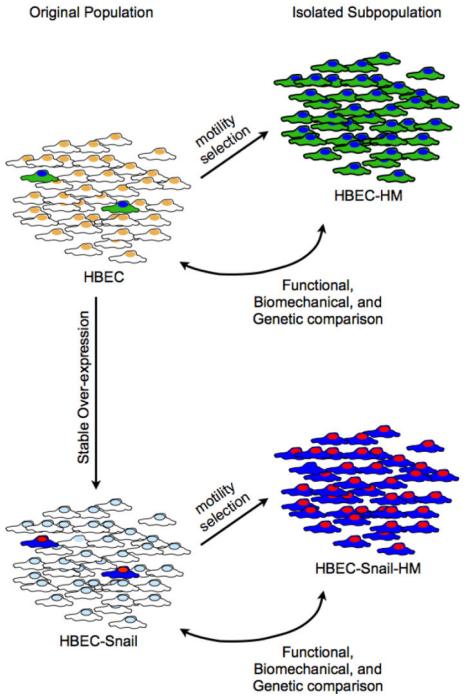

Figure 1.

a: A schematic of the selection process devised for enrichment of highly migratory airway epithelial cells from heterogeneous cultured cell lines. The cells migrated in the absence of chemotactic gradients and were collected from the lower migration chamber. To increase the selection pressure, the cells were serially selected through 8, 5 and then 3 μm pore membranes.

b: Highly migratory subpopulations were isolated from 6 cell lines (3 with and 3 without SNAIL). Double-headed arrows clarify how the functional, biomechanical, and genetic comparisons were made between the original and highly migratory populations.

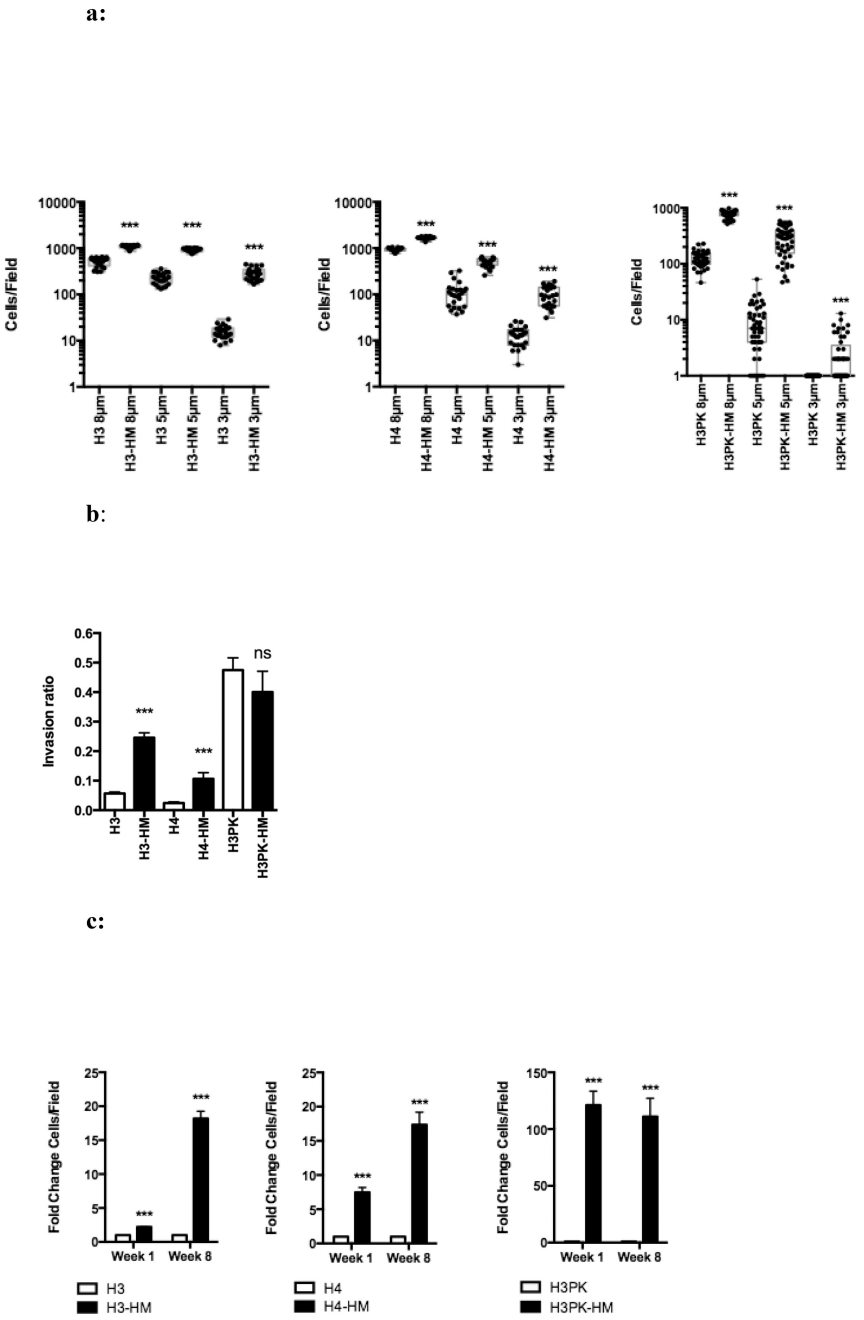

Figure 2.

a: Airway epithelial cells selected through increasingly smaller pores have enhanced migratory capacity. A transwell assay with basal growth medium in both chambers was used to determine cell migration. Migration quantified by fluorescence microscopy and ImageJ of at least 25 fields; each dot represents the number of cells observed in a single field. Mean ± SEM. ***, $P < 0.001$.

b: Highly migratory cells have characteristics that allow for enhanced invasion. The inverted invasion assay shows the invasion ratio (the number of cells invaded divided by number of non-invasive cells). Mean ± SEM. ***, $P < 0.001$.

c: The highly migratory phenotype remains stable eight weeks post-selection. The fold-change in the number of cells/field that migrated to the bottom chamber at week 1 (empty bars) and week 8 (filled bars) after selection and migration through 3 μm pores shown. At least 25 fields were analyzed. Mean ± SEM. ***, $P < 0.001$.

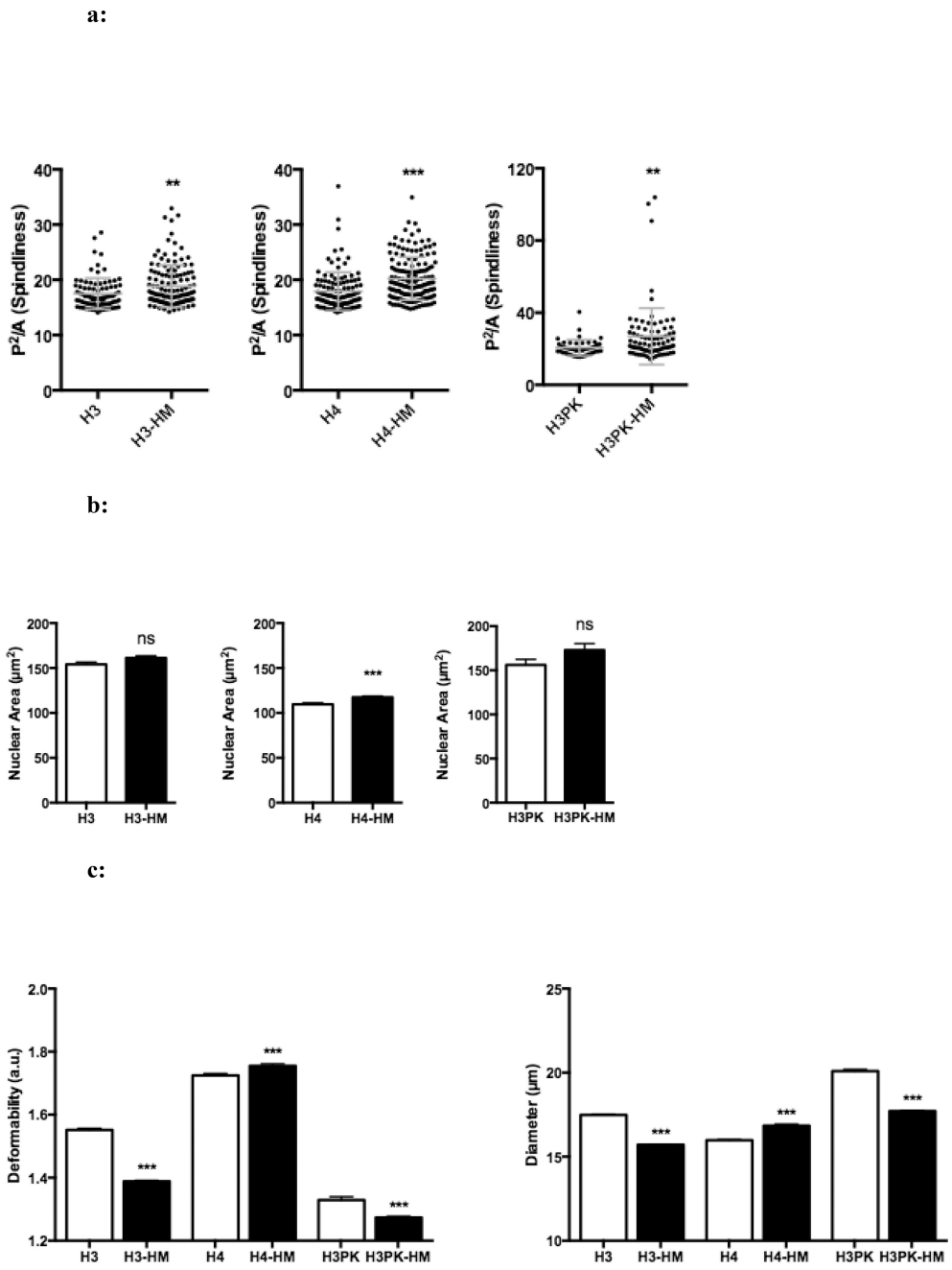

Figure 3.

a: Micropore selection reveals cells having the greatest protrusion intensity. Protrusion intensity, defined as the square of the perimeter divided by area (P2/A) of each cell, was determined using ImageJ. At least 45 cells were analyzed per group; each dot represents the protrusion intensity observed for a single cells. Mean ± SEM. **, P < 0.01; *** P <0.001.

b: Selection does not bias nuclear cross sectional area as determined by post-migration size analysis. Nuclear area was determined by Lamin B1 immunofluorescence of at least 60 cells per group. Mean ± SEM. ***, P < 0.001.

c: Deformability Cytometry (DC) reveals cell line-specific deformability phenotypes coinciding with highly migratory behavior. Graphs show deformability and diameter of at least 1000 unselected and HM cells. Mean ± SEM. *, $P < 0.001$.

a:

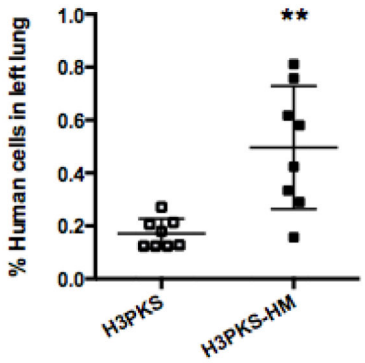

b:

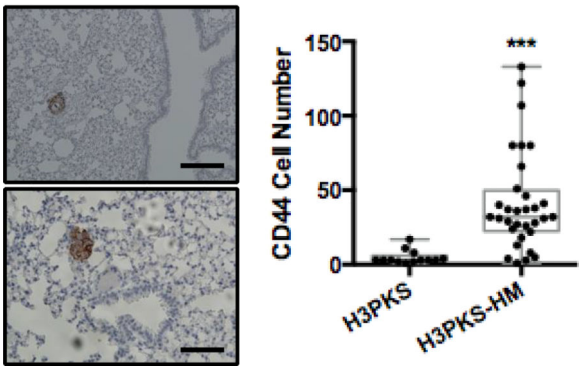

Figure 4.

a: Selected cells show increased persistence in the mouse lung following tail vein injection. H3PKS or H3PKS-HM (5×105) cells were injected intravenously. Lungs were harvested after 72 hours and DNA was extracted. Graph shows qPCR results using human and mouse specific primers. Each dot represents a single mouse; n = 8 mice per group. Mean ± SD. **, $P < 0.01$.

b: Selected cells that survive in the lung parenchyma following tail vein injection are capable of long-term survival and outgrowth as pulmonary premalignant lesions. Lungs were harvested from surviving mice between 26 and 74 days following injection. Right lungs

were stained with a human-specific anti-CD44 antibody to mark the HBECs. n=5 mice in the HM group and n=8 mice in the Control group. Two representative images of the CD44+ HBEC aggregates are shown (left), scale bars are 100 μm. Both images are consistent with premalignant lesions. The number of CD44+ HBEC cells per lesion was quantified manually (right). Each dot represents the number of brown CD44+ HBEC cells comprising a lesion, and every lesion observed was quantitated for every mouse in the group. Mean ± SD. ***, $P<0.001$.

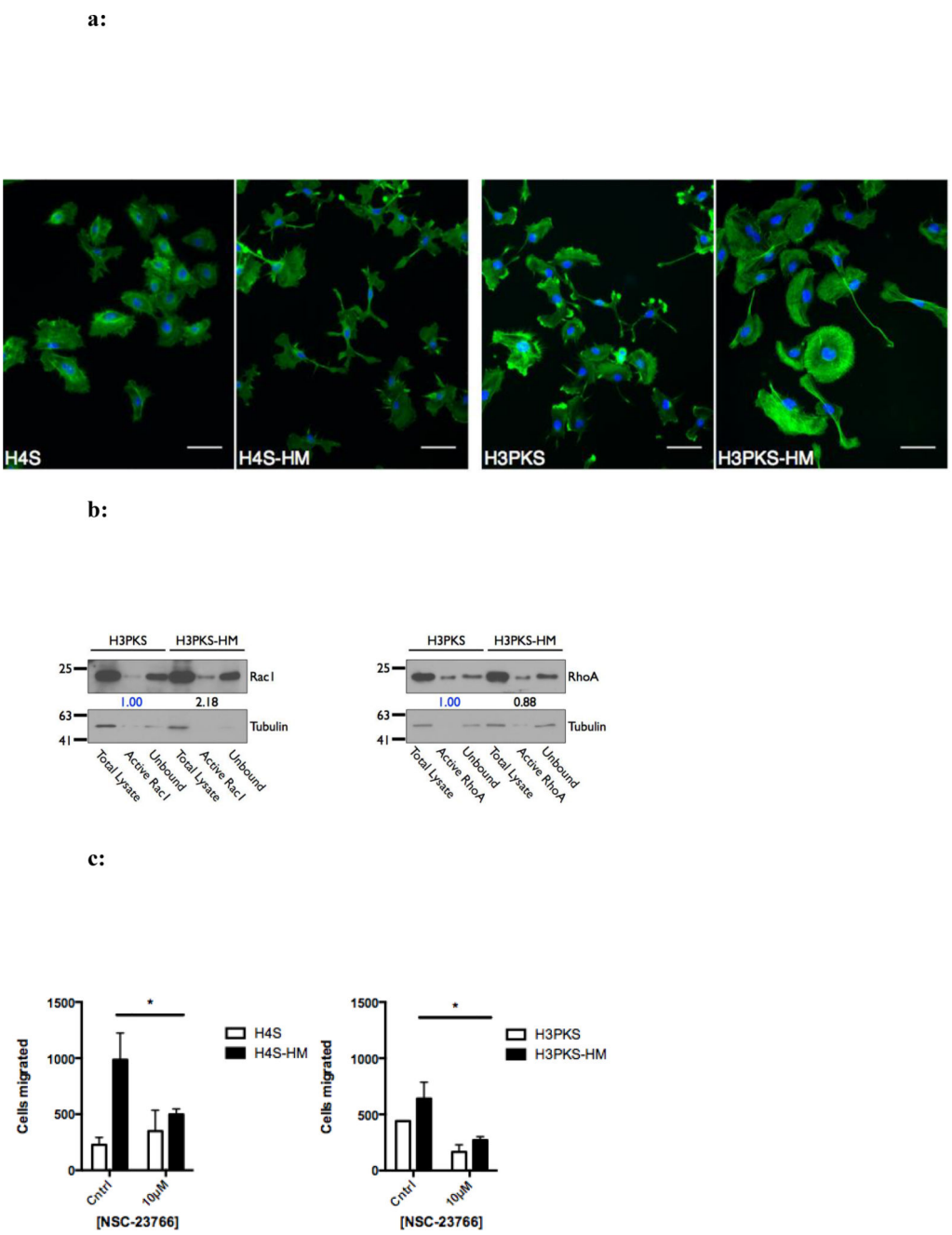

Figure 5.

a: Actin filament structures are abundant in highly migratory cells that express SNAIL. Fluorescence micrographs showing phalloidin-stained F-actin pseudocolored green (nucleus counterstained with DAPI, blue). H3PKS-HM cells have ventral actin-arcs located in the lamellipodia, which are not observed in the unselected cells. H4S-HM cells show long cellular F-actin rich protrusions. 200× total magnification. Scale bar is 50 microns.

b: Highly migratory cells that over-express Snail have increased active Rac1. Western blot and corresponding densitometry showing the relative levels of activated (GTP-bound) RhoA and Rac1 GTPases.

c: High migratory rate facilitated in part through Rac1 activity. Treatment with NSC-23766, an inhibitor of Rac1 activation, perturbs migration through 5 micron pores in highly migratory cells. The absolute number of migrated cells was recorded in replicate wells. Mean ± SEM. *, $P < 0.05$.

a:

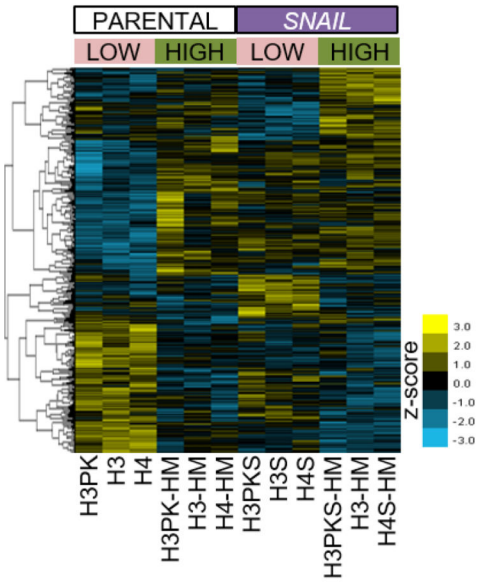

b:

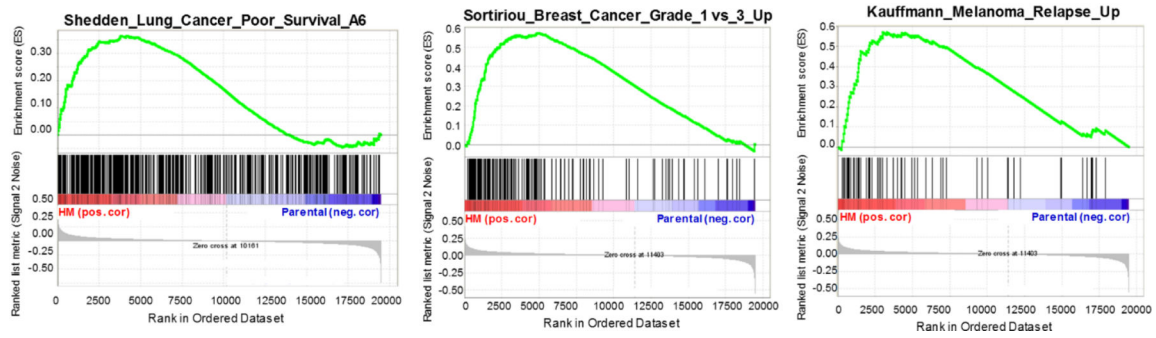

Figure 6.

a: Heat map of gene expression in parental and highly migratory HBECs. The map is organized by parental cell lines (left six columns) and SNAI1 over-expressing cell lines (right six columns), then by low (unselected) versus high migration. This aids in highlighting genes most influenced by migration in SNAI1-dependent and -independent ways.

b: Gene set enrichment analysis reveals correlation between genes associated with high migration rates and poor survival in non-small cell lung cancer and breast cancer or melanoma recurrence. Enrichment plot of two gene sets significantly (false discovery rate q-

value < 0.01) associated with high mobility SNAI1 HBECs as compared to non-selected parental cell lines.